MINISTRY OF EDUCATION AND TRAINING

VIETNAM ACADEMY OF SCIENCE AND TECHNOLOGY

GRADUATE UNIVERSITY OF SCIENCE AND TECHNOLOGY

Mai Thi Xuan

INVESTIGATION OF COPPER/IRON-BASED CATALYSTS WITH CHALCOGENS (O, S) FOR ELECTROCHEMICAL CO_2 REDUCTION REACTIONS

SUMMARY OF DISSERTATION ON SCIENCES OF MATTER

Major : Theoretical and physical chemistry

Code: 9440119

Hanoi - 2026

The dissertation is completed at: Graduate University of Science and Technology, Vietnam Academy of Science and Technology

Supervisor 1: Dr. Le Thi Ly
Supervisor 2: Prof.Dr. Luc Huy Hoang

Reviewer 1:
Reviewer 2:
Reviewer 3:

The dissertation is examined : by Examination Board of Graduate University of Science and Technology, Vietnam Academy of Science and Technology at.

The dissertation can be found at:
- Library of Graduate University of Science and Technology
- National Library of Vietnam

INTRODUCTION

Nowadays, global energy consumption has rapidly increased due to the economic and technology development. Fossil fuels remain the primary energy source, and their consumption causes severe environmental issues, such as excess CO_2 emission driving the greenhouse effect and alarming climate change. Therefore, finding methods to reduce excess CO_2 is essential and extremely urgent. In recent years, CO_2 reduction has been investigated via thermochemical, photochemical, and electrochemical pathways. Among these, the electrochemical CO_2 reduction method has drawn the most scientific attention due to its distinct advantages, including mild reaction conditions operating at room temperature and ambient pressure. Furthermore, both the reaction rate and product selectivity can be precisely controlled by adjusting the applied potential and tuning the catalyst. This approach holds strong potential for wide-scale application through the design of electrolyzers, which can be easily coupled with renewable energy sources (such as solar or wind power) to effectively utilize surplus electricity. These advantages position electrochemical CO_2 reduction as a highly promising strategy to boost renewable energy integration in the chemical and fuel industries.

The efficiency of electrochemical CO_2 reduction heavily relies on the nature of the heterogeneous catalyst employed at the electrode. To date, numerous heterogeneous catalysts have been investigated for this reaction, which can be generally categorized into four groups based on their product distribution: (1) Au, Ag, Zn, Pd, and Ga, which exhibit moderate binding affinity for *CO intermediates, allowing CO gas desorption from the surface; (2) Pb, Hg, In, Sn, Cd, and Bi, which interact weakly with *CO but stabilize the *OCHO intermediate, leading to formate as the primary product; (3) Ni, Fe, Pt, and Ti, which bind strongly to hydrogen atoms (H), making the competitive hydrogen evolution reaction (HER) dominant and drastically lowering CO_2 reduction efficiency. Cu stands out as the only metal discovered so far capable of reducing CO_2 into multi-carbon hydrocarbons and alcohols (such as ethylene and ethanol) with significant efficiency. This capability is attributed to Cu's binding affinity for *CO intermediates, which is strong enough to drive further reduction steps (forming *CHO or *COH) and enable C-C coupling rather than immediate CO release. This versatility

in generating diverse products, from hydrocarbons to organic acids, makes Cu-based catalysts ideal subjects of research and positions them among the premier materials for CO_2 reduction in aqueous electrolytes. Nevertheless, metallic Cu catalysts still suffer from drawbacks, including suboptimal product selectivity (often yielding a complex mixture), poor long-term stability, and efficiencies that fall short of commercial requirements. To overcome these limitations, a prominent and highly active research direction in recent years focuses on modifying Cu-based materials by integrating chalcogen elements (O, S) or pairing them with another metal alongside chalcogens to induce synergetic effects (such as $Cu_xFe_{3-x}O_4$). These catalytic materials exhibit excellent electrochemical activity, good electrical conductivity, and high power capability. Consequently, materials containing copper and chalcogens represent highly efficient catalysts for electrochemical CO_2 reduction and hold great promise for future practical applications.

In Vietnam, while awareness of climate change and the need for energy transition is growing, fundamental and in-depth research on electrochemical CO_2 reduction—particularly catalyst material development—remains limited. Most domestic studies have only advanced to product prediction without definitive product analysis or catalyst selectivity evaluation. Synthesizing materials, systematically assessing catalytic efficiency, and especially performing qualitative and quantitative analysis of the resulting products to determine selectivity, still represent a significant research gap. Driven by these practical needs and academic challenges, we selected the dissertation topic: **"Investigation of Copper/Iron-based catalysts with Chalcogens (O, S) for Electrochemical CO_2 reduction reactions"**.

Research objectives of the dissertation:

1. Successfully synthesize CuO oxide, spinel $Cu_xFe_{3-x}O_4$ oxide ($0 < x < 3$), and CuS materials.
2. Evaluate the activity of each catalyst type for the electrochemical CO_2 reduction reaction, accurately quantify the formed products, and determine the selectivity of each catalyst toward specific products.

3. Elucidate the structural and morphological transformations of the catalysts after electrolysis, and propose the active catalytic sites for the CO_2 reduction reaction on the investigated electrodes.

Research content of the dissertation:

Based on the objectives above, the dissertation covers the following research scopes:

Content 1: Synthesis and characterization of nanostructured CuO, $Cu_xFe_{3-x}O_4$ ($0 < x < 3$), and CuS materials.

- Synthesize CuO and $Cu_xFe_{3-x}O_4$ ($0 < x < 3$) catalysts via the sol-gel method.
- Synthesize CuS catalysts via the solvothermal method.
- Investigate the structure and morphology of the catalysts using physicochemical analytical methods.

Content 2: Investigation of the electrochemical properties of the catalyst materials for the CO_2 reduction reaction.

- Evaluate electrochemical performance using CV, LSV, and CA methods.
- Examine product selectivity under various applied potentials.

Content 3: Study of the reaction mechanism of CO_2 reduction through post-electrochemical structural and morphological assessments.

- Analyze the physicochemical properties of the post-catalytic materials.
- The active catalytic sites for the electrochemical CO_2 reduction reaction.

Scientific and practical basis of the topic:

The practical basis of this dissertation rests on a solid methodological framework aimed at transforming CO_2 - a major greenhouse gas driving climate change - into valuable products, thereby contributing to the development of circular carbon economy technologies and emission reduction. Drawing from established scientific principles of electrochemical CO_2 reduction, the dissertation applies the following strategies: (1) Targeted synthesis of copper-based materials (the top-performing heterogeneous catalyst class for electrochemical CO_2 reduction) by preparing CuO and $Cu_xFe_{3-x}O_4$ via the sol-gel method and CuS via the solvothermal method; (2)

Evaluation of electrochemical CO_2 reduction performance by combining electrochemical measurements with product analysis via gas chromatography (GC) and ion chromatography (IC) to clarify selectivity. This allows for the calculation of the Faradaic efficiency (FE) of products to validate their practical viability; (3) Mechanistic insights gained by examining the post-reaction materials using XRD, EDX, SEM, and EDS mapping to the active catalytic sites. This provides fundamental guidelines for designing next-generation catalysts for more effective carbon capture and utilization.

CHAPTER 1. OVERVIEW

1.1. General background of electrochemical CO_2 reduction catalysis

The CO_2 reduction reaction is a multi-electron process involving the transfer of $2e^-$, $4e^-$, $6e^-$, or $8e^-$. The combination of these electrons with corresponding protons yields a variety of products. The reaction takes place within an electrolyzer featuring separate anodic and cathodic compartments divided by a membrane. At the anode, water is oxidized to generate oxygen gas. At the cathode, CO_2 molecules undergo reduction into diverse chemical species. Since this is an endergonic process, an external electrical potential must be supplied. The thermodynamic potential for the single-electron reduction of CO_2 to form the radical intermediate $*CO_2^-$ is highly unfavorable at -1.49 V *vs.* RHE, demanding significant energy. Conversely, multi-electron pathways reducing CO_2 to products like CO, HCOOH, CH_4, and CH_3OH exhibit equilibrium potentials (E_0) clustered tightly between 0.169 V and -0.025 V *vs.* RHE. These close thermodynamic values usually lead to poor product selectivity. Therefore, a major bottleneck in electrochemical CO_2 reduction is designing highly selective catalysts capable of suppressing undesirable side reactions.

1.2. Overview of catalyst materials for CO_2 reduction

Among pristine metal catalysts, Cu is uniquely capable of binding and converting *CO intermediates into high-value hydrocarbons or alcohols. However, metallic copper requires high overpotentials for CO_2 reduction (close to -1 V), which compromises overall energy efficiency. Furthermore, pristine Cu electrodes suffer from rapid deactivation over extended electrolysis periods, posing a major barrier to commercial adoption.

Transition metal chalcogenides, mixed metal oxides, and spinels have emerged as key strategies to enhance performance by combining the strengths of two distinct metals to modulate electronic conductivity and surface morphology. Nevertheless, deploying these complex compounds for CO_2RR still faces issues in managing composition and structural integrity to achieve high efficiency paired with long-term stability.

1.3. Research background in worldwide and Vietnam

Globally, numerous research groups are actively exploring electrochemical CO_2 reduction catalysis, with several systems approaching pilot-scale implementation. In Vietnam, however, basic and comprehensive research in this field-especially regarding novel catalyst design-remains scarce. Most domestic efforts rely on theoretical product predictions without executing rigorous product quantification or selectivity assays. Synthesizing these materials, evaluating their catalytic pathways systematically, and performing qualitative and quantitative tracking of the resulting products to establish selectivity maps represents an unaddressed gap in the domestic literature.

CHAPTER 2. EXPERIMENT AND RESEACH METHODS

2.1. Experimental

2.1.1. Synthesis of CuS material by the solvothermal method

Procedure: 2 mmol of thiourea were added to 60 mL of ethane-1,2-diol (solution 1). Subsequently, 1 mmol of $Cu(NO_3)_2 \cdot 3H_2O$ was added to solution 1, and the mixture was stirred at room temperature for 30 minutes. The mixture was transferred into a hydrothermal autoclave and heated at different temperatures (120, 150, 180 °C) for 24 hours. After cooling to room temperature, the product was washed and centrifuged three times with EtOH. The obtained solid was vacuum-dried at 60 °C overnight to yield the final product.

2.1.2. Synthesis of CuO and $Cu_xFe_{3-x}O_4$ (CFO-x) (x = 0.5, 1, 1.5, 2) materials by the sol-gel method

HNO_3 was added to 100 mL of H_2O, then 1 g of agar was added, and the mixture was stirred and heated to 80 °C (solution 1). A second solution containing $Cu(NO_3)_2$ and $Fe(NO_3)_3$ in the desired molar ratio was prepared

in 100 mL of H_2O and stirred until the salts were completely dissolved (solution 2). Solution 2 was poured into solution 1 to form a sol, and stirring was continued for 3 h at 80 °C to obtain a gel. The gel was dried at 100 °C, ground into a powder, and then calcined at different temperatures in air to obtain the product. For the synthesis of CuO alone, no $Fe(NO_3)_3$ was added.

2.2. Physicochemical characterization methods

- X-ray diffraction (XRD) was performed on a D8-ADVANCE (Germany) diffractometer.
- Raman spectroscopy was performed on a LabRAM HR Evolution (HORIBA Scientific, Japan) spectrometer.
- X-ray photoelectron spectroscopy (XPS) was performed on an ESCALab 250 (Thermo Scientific, USA) spectrometer.
- Fourier-transform infrared (FT-IR) spectroscopy was performed on a FTIR Nexus 670 (USA) spectrometer.
- Scanning electron microscopy (SEM) and energy-dispersive X-ray spectroscopy (EDS) were performed on a FE-SEM Hitachi S-4800 (Japan) microscope.
- Transmission electron microscopy (TEM) and high-resolution transmission electron microscopy (HR-TEM) were performed on a JEM 2100 (JEOL, Japan) microscope.

2.3. Electrochemical measurement methods

Electrochemical experiments to investigate the electrochemical properties and catalytic activity of the catalysts for the CO_2 reduction reaction were performed on a BioLogic SP 50 or SP 300 (France) electrochemical workstation. The electrochemical measurements included:
- Linear sweep voltammetry (LSV).
- Chronoamperometry (CA).

CHAPTER 3. RESULTS AND DISCUSSION

3.1. Investigation of CuO catalyst material

3.1.1. X-ray diffraction (XRD) of the CuO material

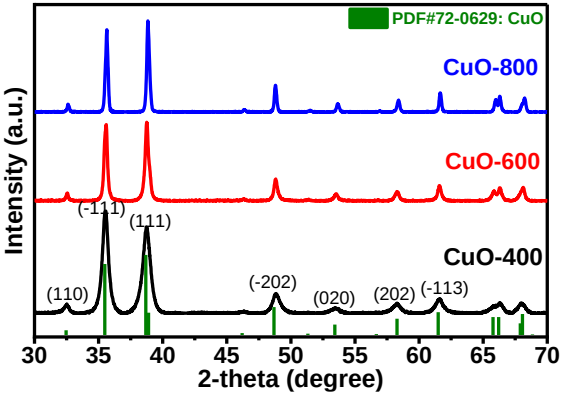

Figure 3.1. *X-ray diffraction pattern of the CuO material*

Figure 3.1 presents the X-ray diffraction patterns of the CuO samples calcined at 400, 600, and 800 °C. The diffraction peaks of all three samples are consistent with the standard PDF card No. 01-085-7183, confirming the formation of the monoclinic CuO phase. From the XRD patterns, the crystallite sizes estimated using the Scherrer method are approximately 15 nm (400 °C), 17 nm (600 °C), and 31 nm (800 °C); that is, as the calcination temperature increases from 400 to 800 °C, the crystallite size approximately doubles. These results indicate that the CuO material was successfully synthesized and that the crystallite size increases with the heat treatment temperature.

3.1.2. Raman spectroscopy of the CuO material

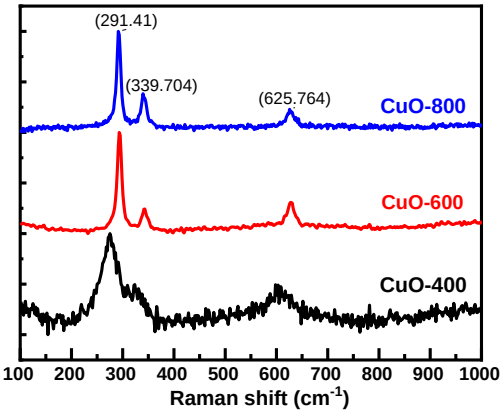

Figure 3.2. *Raman spectroscopy of the CuO material*

Figure 3.2 presents the Raman spectroscopy of the CuO samples calcined at 400, 600, and 800 °C. All three samples exhibit three characteristic peaks at approximately 292, 339, and 625 cm^{-1}, assigned to the Cu–O vibrations of monoclinic CuO. The CuO-400 sample shows broader and less sharp peaks compared to CuO-600 and CuO-800, reflecting its lower crystallinity / smaller crystallite size and/or higher defect density. Comparison with the Raman scattering spectroscopy of CuO samples reported in the literature (peaks at ~295, ~343, and ~630 cm^{-1}) shows good agreement in peak positions. Together with the XRD results, this confirms that CuO was successfully synthesized at all three calcination temperatures (400, 600, 800 °C).

3.1.3. Scanning electron microscopy (SEM) of the CuO material

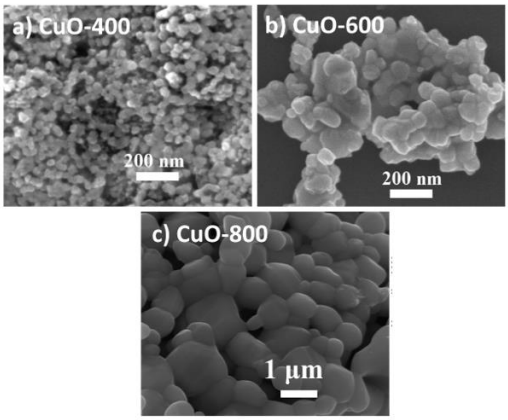

Figure 3.3. *Scanning electron microscopy (SEM) of the CuO material*

Analysis of scanning electron microscopy (SEM) images of the CuO materials revealed differences in morphology among the CuO samples calcined at different temperatures. Increasing the calcination temperature led to a corresponding increase in particle size. The particle size of each material was determined using ImageJ software by measuring individual particles on the SEM images and then calculating the average size. The CuO-400 sample exhibited an average particle size of 33 ± 4 nm. When the calcination temperature was increased to 600 °C, CuO-600 showed an average size of 81 ± 10 nm. At a calcination temperature of 800 °C, the CuO-800 sample had an average particle size of 824 ± 127 nm. This morphological analysis

demonstrates that the calcination temperature significantly affects the particle size of the CuO material, with higher calcination temperatures leading to a substantial increase in particle size.

3.1.4. Investigation of the electrocatalytic activity for CO_2 reduction

3.1.4.1. Linear sweep voltammetry (LSV) of the CuO material

To evaluate the CO_2 reduction activity, the first measurement employed was linear sweep voltammetry (LSV). This technique allows the determination of reduction reactions occurring at the electrode and enables the identification of the onset overpotential, thereby facilitating the selection of a suitable electrolysis potential for the CuO material.

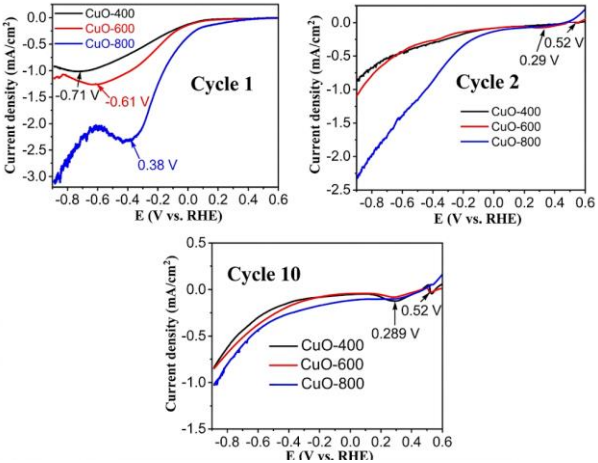

Figure 3.4. *LSV results of the CuO material system at cycles 1, 2, and 10 in CO_2-saturated 0.1 M $NaHCO_3$ solution (pH = 6.8) at a scan rate of 5 mV/s in the potential range from 0.6 to –0.9 V vs. RHE.*

In previous studies, CuO typically exhibits two redox pairs Cu^{II}/Cu^{I} and Cu^{I}/Cu^{0} in the range of 0.56-0.1 V *vs.* RHE, occurring prior to the CO_2 reduction catalytic current region. In cycle 1 (Figure 3.4), the CuO-400 sample shows a broad reduction peak starting at ~0.10 V and reaching a maximum at -0.71 V *vs.* RHE; the broadness of the peak suggests the reduction process CuO → Cu. The CuO-600 and CuO-800 samples have similar onset potentials, but their peak maxima are shifted anodically, at -0.61 V and -0.38 V *vs.* RHE, respectively. This shift is consistent with the

increase in calcination temperature, which enhances the crystallinity/conductivity of CuO and may be further assisted by residual electrically conductive carbon remaining after calcination. From cycle 2 onward, the peaks at -0.71/-0.61/-0.38 V disappear. Instead, CuO-400 and CuO-600 exhibit peaks at approximately 0.50 and 0.30 V, characteristic of the sequential reduction steps $Cu^{2+} \rightarrow Cu^{+}$ and $Cu^{+} \rightarrow Cu^{0}$. For CuO-800, these peaks are no longer observed, indicating that the surface is reduced to Cu^{0} already in the first cycle. By cycle 10, these peaks shift slightly (≈0.52 and 0.289 V) and the catalytic current density decreases compared to cycle 2, reflecting a loss of activity during reconstruction/reduction. At -0.90 V *vs.* RHE in cycle 10, CuO-800 gives the highest current density of ~1 $mA.cm^{-2}$. When the catalytic current has stabilized (cycle 10), the onset potential lies around -0.50 V *vs.* RHE; therefore, potentials of -0.60, -0.70, -0.80, and -0.90 V *vs.* RHE were selected for electrolysis to evaluate the product selectivity of CO_2RR on the CuO electrodes.

3.1.4.2. Product selectivity of the CO_2 reduction reaction on the CuO material

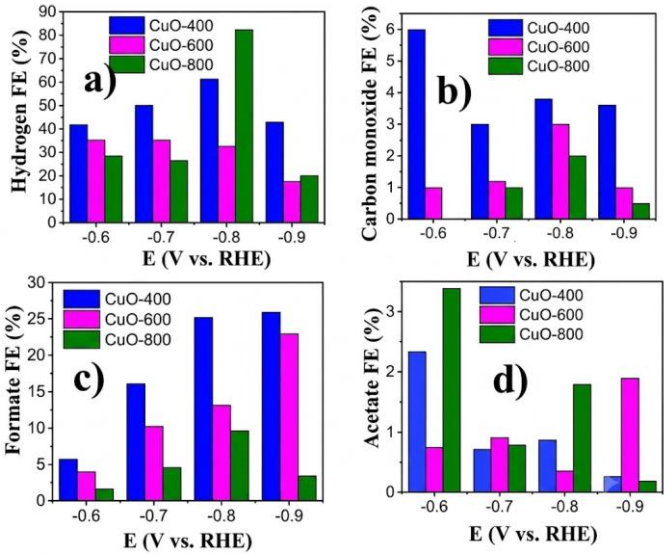

Figure 3.5. *Faraday efficiency of the CuO material system in CO_2-saturated 0.1 M $NaHCO_3$ solution (pH = 6.8) at potentials from -0.6 V to -0.9 V vs. RHE for the products of electrochemical CO_2 reduction: a) Hydrogen, b) CO, c) $HCOO^-$, d) CH_3COO^-.*

Gas products quantified by GC showed that CO_2RR produced a mixture of H_2 and CO (Figure 3.5 a,b). At all examined potentials, H_2 was the predominant product with an average Faraday efficiency (FE) of ~49%, while CO reached only 3-6%. No CH_4 or C_2H_6 was detected, in contrast to some previous reports. For the liquid phase (analyzed by ion-exchange chromatography), formate ($HCOO^-$) and acetate (CH_3COO^-) were the two main products. Acetate was formed at all potentials but with low FE; the highest value (~3.8%) was obtained at -0.6 V *vs.* RHE for the CuO-400 sample. Formate was also present across the entire potential range and increased markedly at -0.7, -0.8, and -0.9 V *vs.* RHE; notably, at -0.9 V *vs.* RHE, CuO-400 achieved a formate FE of approximately 26%. A comparison among the samples reveals that, under identical potential conditions, CuO-400 consistently exhibited a higher formate FE than CuO-600 and CuO-800.

3.1.5. Morphological and structural characterization of the CuO material after CA

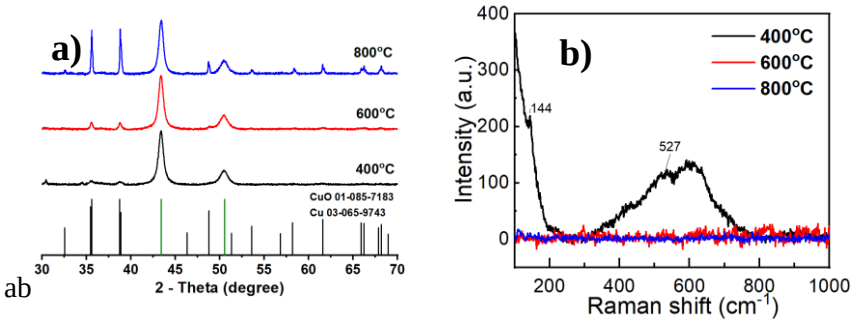

Figure 3.6. *X-ray diffraction patterns and Raman spectroscopy of the CuO material after 2 h of electrolysis at –0.8 V vs. RHE in CO_2-saturated 0.1 M $NaHCO_3$ solution.*

Figure 3.6 a (XRD) shows that after electrolysis, the CuO-800 sample still retains the characteristic peaks of pristine CuO while two new peaks corresponding to metallic Cu (111) and (200) appear, indicating partial reduction of CuO → Cu. In contrast, for CuO-400 and CuO-600, the metallic Cu peaks are sharp while the CuO signals almost disappear, suggesting that CuO has been reduced nearly completely to Cu. The “preservation” of the CuO phase in CuO-800 may originate from the high calcination temperature, which increases crystallinity and reduces grain boundary density, making the

structure more resistant to phase transformation under reductive potential. However, this high crystallinity is detrimental to CO_2RR because it hinders the formation of Cu^0—the phase considered to be the true catalytically active site. None of the three samples showed Cu_2O peaks in XRD. Nevertheless, Figure 3.6 b (Raman scattering spectroscopy) records characteristic vibrations of Cu_2O only for the CuO-400 sample. This is consistent with reports showing that metallic Cu can be re-oxidized to Cu_2O after the reductive potential is removed. We attribute this to the higher particle/surface boundary density of the CuO-400 sample, which makes it more chemically active, facilitating oxygen diffusion to the surface and Cu oxidation. In contrast, for CuO-600 and CuO-800, the lower particle density and larger crystallite size (as calculated from XRD) limit post-electrolysis oxidation, so no Cu_2O signal is observed in the Raman scattering spectroscopy. Studies on copper oxide catalysts after electrochemical reduction show that they transform into metallic Cu but are also easily oxidized to Cu_2O when the reductive potential is no longer applied. This is believed to be due to the high density of interconnected particles, which makes them more chemically active and may enable oxygen to diffuse more effectively to the surface. The Cu particles in the CuO-600 and CuO-800 samples, having larger crystallite sizes and thus lower particle density, are not oxidized to Cu_2O.

3.2. Investigation of $Cu_xFe_{3-x}O_4$ (CFO) catalyst material

3.2.1. X-ray diffraction (XRD) of the CFO material

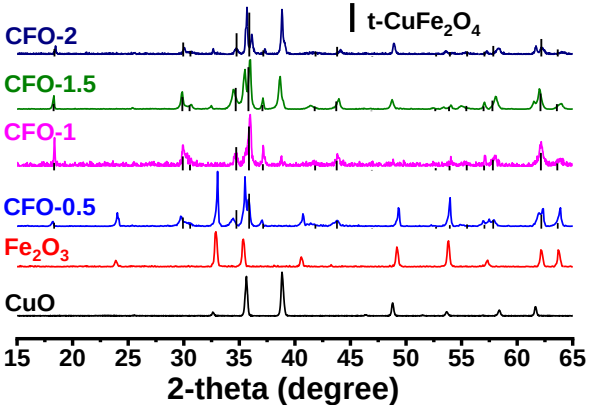

Figure 3.7. *X-ray diffraction pattern of the CFO material*

The results in Figure 3.7 show that each CFO material consists of spinel and simple oxide phases with different percentages, depending on the initial precursor molar ratio used in the synthesis. For CFO-0.5, with a Cu/Fe molar ratio of 1/5 (the Fe precursor amount is five times that of Cu), the obtained product contains, besides the spinel phase (which exhibits a tetragonal crystal system), an additional Fe_2O_3 simple oxide component (Figure 3.7, CFO-0.5 curve, blue). When the Cu molar ratio increases, CFO-1 (Cu/Fe = 1/2) gives the highest proportion of the $CuFe_2O_4$ spinel product, with no residual Fe_2O_3 (all Fe is incorporated into the spinel), but a small amount of excess CuO remains. Upon further increasing the Cu precursor concentration to equimolar with Fe (Cu/Fe = 1/1), since Fe_2O_3 had already been fully consumed at the previous ratio, the excess simple oxide at this 1/1 ratio is still CuO but with a larger amount, qualitatively reflected by the higher diffraction peak intensity in Figure 3.7 (CFO-1.5 curve, green). Finally, when the Cu precursor concentration is twice that of Fe (Cu/Fe = 2/1), the amount of excess simple oxide increases further, as evidenced by the even higher intensity of the CuO diffraction peaks (Figure 3.7, CFO-2 curve, navy blue).

3.2.2. SEM, TEM and EDX analysis of the CFO spinel material

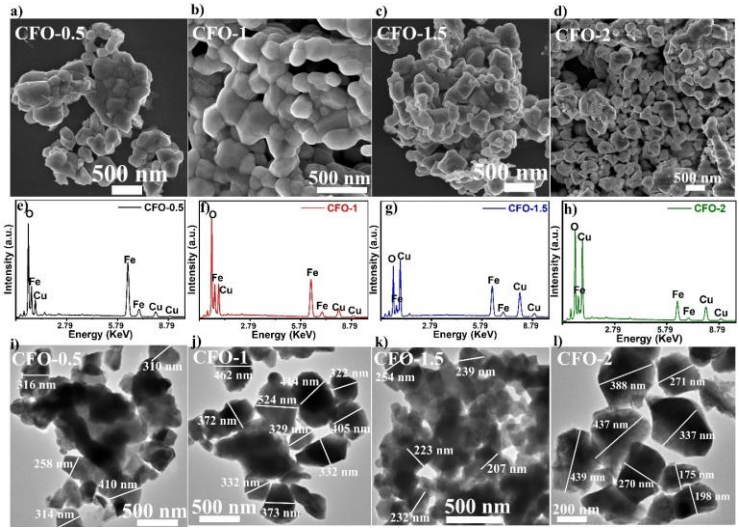

Figure 3.8. *Scanning electron microscopy (SEM) images, energy-dispersive X-ray spectroscopy (EDX) spectroscopy, and transmission electron microscopy (TEM) images of the CFO material.*

The morphology, particle size, and elemental composition of the CFO material system were investigated using scanning electron microscopy, transmission electron microscopy, and energy-dispersive X-ray spectroscopy. The results are presented in Figure 3.8. The SEM images of the CFO materials (Figure 3.8, a-d) show good crystallinity for all four CFO samples, with well-defined crystals, clear grain boundaries, and relatively uniform particle sizes. Although the phase composition was clearly identified by XRD, the SEM images alone cannot distinguish the different CFO samples because the particle sizes are relatively uniform after calcination. The EDX spectroscopy (Figure 3.8, e-h) reveal that the CFO materials contain Cu, Fe, and O. The TEM images show relatively large particles in the size range of 200-500 nm. Due to this large particle size, lattice fringes could not be observed to determine the interplanar spacing.

3.2.3. Product selectivity of the reduction process on the CFO material

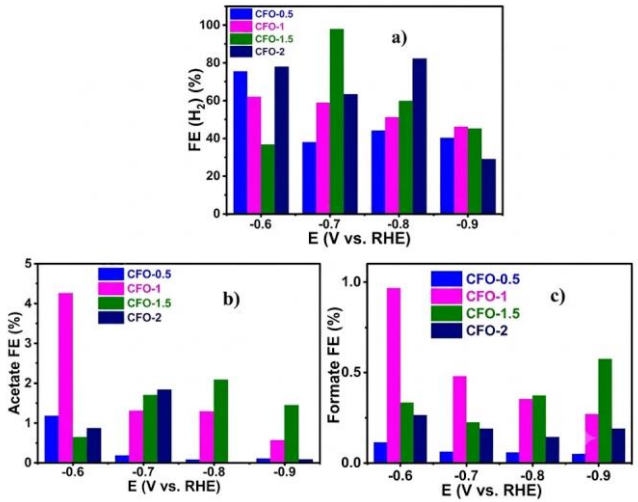

Figure 3.9. *Faraday efficiency of gaseous and liquid products on the CFO material after 2 h of potentiostatic electrolysis at potentials ranging from –0.6 to –0.9 V vs. RHE in CO_2-saturated 0.1 M $NaHCO_3$ solution (pH = 6.8).*

The results in Figure 3.9 show that during catalytic operation, the CFO materials produced three products: gaseous hydrogen and liquid acetate and formate. The bar charts for each product at different potentials allow comparison of the product performance on the CFO materials at each applied

potential. The Faraday efficiency plots for hydrogen show that all four CFO electrodes generate hydrogen at all potentials with high efficiency, notably the CFO-1 electrode, which exhibits a hydrogen evolution efficiency above 80%. The CFO-0.5 electrode maintains a stable hydrogen Faraday efficiency of about 40% at higher potentials, except at the low potential of -0.6 V *vs.* RHE, where the efficiency reaches nearly 80%. Since electrochemical CO_2 reduction is always accompanied by the competing proton reduction reaction (HER), the Faraday efficiency of hydrogen gas is consistently high. The Faraday efficiency of H_2 shown in Figure 3.9 a reaches approximately 100% for the CFO-1 and CFO-1.5 electrodes at -0.6 and -0.7 V *vs.* RHE. The CFO-0.5 and CFO-2 electrodes also achieve hydrogen evolution efficiencies of up to about 80%. For all four CFO electrodes, no CO product was detected among the gaseous products at any of the applied potentials.

3.2.4. Morphological and structural characterization of the CFO material after catalytic operation

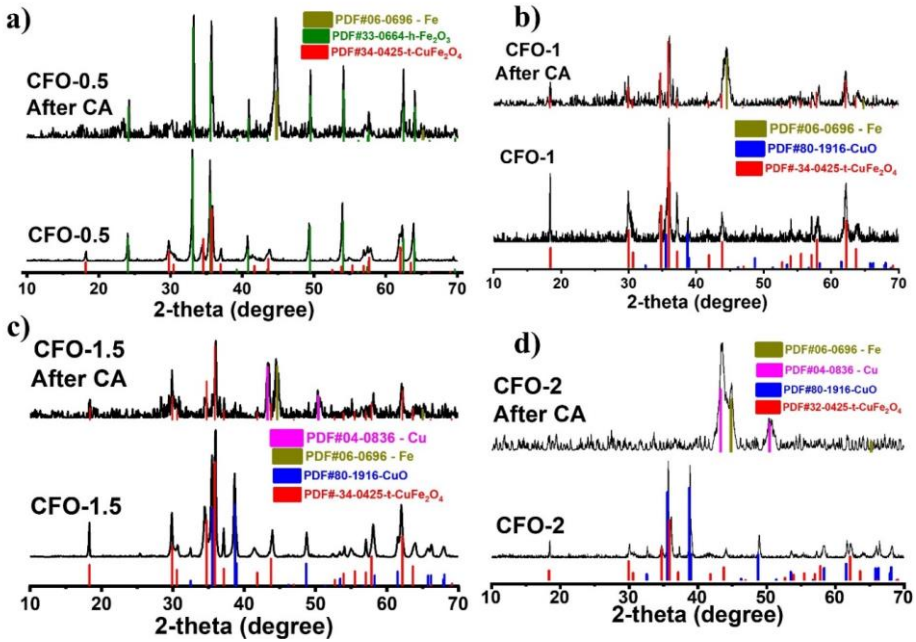

Figure 3.10. X-ray diffraction patterns of the CFO material before and after 2 h of electrolysis at -0.6 V vs. RHE in CO_2-saturated 0.1 M $NaHCO_3$ solution (pH = 6.8).

After 2 hours of continuous catalytic operation at -0.6 V *vs.* RHE, the phase composition of each CFO material changed significantly compared to the pristine CFO. On the CFO-1 electrode, which initially consisted of $CuFe_2O_4$ (83.8%) and CuO (16.2%), the diffraction peaks of CuO disappeared after catalysis, while $CuFe_2O_4$ still remained and additional peaks of metallic Fe appeared (Figure 3.10 b). The emergence of metallic Fe after electrochemical operation indicates that the $CuFe_2O_4$ spinel was reduced to the zero-valence metal; CuO was also reduced to metallic Cu, but the small initial amount of CuO meant that Cu peaks were not detectable in the XRD pattern (Figure 3.10 b). Indeed, for the CFO-1.5 and CFO-2 electrodes, which contained higher amounts of CuO (39.6% for CFO-1.5 and 48.9% for CFO-2), the CuO diffraction peaks disappeared after catalysis (Figures 3.10 c,d) and were replaced by peaks of metallic Cu. Because the spinel $CuFe_2O_4$ content was higher on CFO-1.5 (60.4%) than on CFO-2 (51.1%), after catalytic operation all of the $CuFe_2O_4$ on CFO-2 was reduced to metallic Fe, whereas on CFO-1.5 both $CuFe_2O_4$ and metallic Fe remained. These results further confirm that the catalytic process reduces $CuFe_2O_4$ spinel to metallic Fe and CuO to metallic Cu. The residual $CuFe_2O_4$ after catalysis may correspond to the portion of the material that was not in contact with the electrolyte during operation. For the CFO-0.5 electrode, which initially consisted of $CuFe_2O_4$ (33.2%) and Fe_2O_3 (66.8%), after catalysis the spinel component was completely reduced to metallic Fe, while characteristic diffraction peaks of Fe_2O_3 were still observed (Figure 3.10 a).

From the XRD analysis of the CFO electrodes after catalytic operation, combined with the gaseous and liquid products obtained after electrolysis, the results show that the materials on the electrodes were reduced to metallic Cu and Fe during catalysis. The thesis also consulted previously published references to indirectly draw conclusions about the CFO material. A study published in 2015 in *ACS Catalysis* by Jian Zhao and co-workers demonstrated that Cu nanoparticles derived from the reduction of Cu_2O are efficient electrocatalysts for the proton reduction reaction (HER) in a neutral electrolyte (pH 7). Another study reported that the active site for HER in alkaline medium is the single-crystalline $Fe–N_x$ material, where the single Fe site with more d-electrons is more favorable for H_2 evolution. Among the CFO spinel electrodes, the residual $CuFe_2O_4$ spinel phase after electrochemical operation was most clearly observed on CFO-1 and

CFO-1.5; these two electrodes also produced larger amounts of liquid acetate than the other electrodes. This indicates that the spinel oxide is the material responsible for CO_2 reduction to acetate.

3.3. Investigation of CuS catalyst material

3.3.1. X-ray diffraction (XRD) of the CuS material

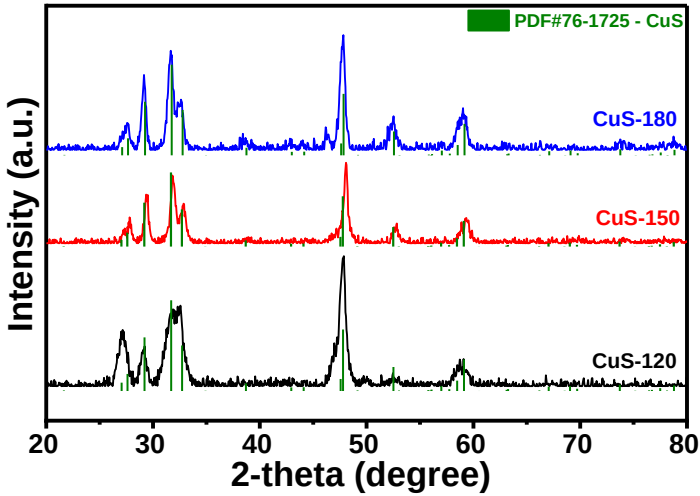

Figure 3.11. *X-ray diffraction patterns of the CuS samples prepared at different solvothermal temperatures (120, 150, 180 °C).*

Figure 3.11 shows the X-ray diffraction (XRD) patterns of the CuS samples prepared at different solvothermal temperatures (120, 150, and 180 °C). The results indicate that all three synthesis temperatures yield products with the CuS structure, as the diffraction peaks match the standard PDF card No. 76-1725. The samples differ in lattice parameters and crystallite size. At a solvothermal temperature of 120 °C, the crystallite size is the smallest (7 nm), with lattice parameters a = 0.3794 nm and c = 1.646 nm. At 150 °C and 180 °C, the obtained crystallite sizes are relatively similar, namely 15 nm and 16 nm, respectively. The lattice parameters calculated for CuS-150 are a = b = 0.37915 nm, c = 1.64135 nm; for CuS-180, a = 0.38174 nm, c = 1.60643 nm. This variation can be explained by the fact that increasing the solvothermal temperature leads to a higher crystal growth rate, resulting in larger crystallite sizes compared to those obtained at lower temperatures.

3.3.2. Raman spectroscopy analysis of the CuS material

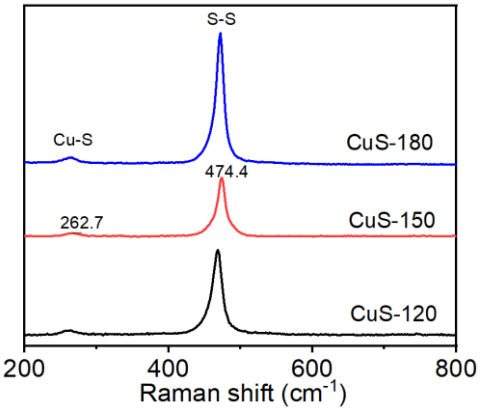

Figure 3.12. *Raman spectroscopy of CuS materials synthesized by the solvothermal method at different temperatures (120, 150, 180 °C).*

The Raman spectroscopy of the CuS materials were recorded using a 532 nm laser. As shown in Figure 3.12, two Raman shifts at 264 and 474 cm^{-1} were observed for all three samples. Comparison with the CuS material synthesized by Karikalan and co-workers also shows peaks at 264 and 474 cm^{-1}, which correspond to the characteristic Cu–S and S–S bonds, respectively, in the CuS crystal. The XRD and Raman results confirm the successful synthesis of the CuS material.

3.3.3. SEM, TEM, and HRTEM analysis of the CuS material

SEM images (Figure 3.13 a-c) show that all three samples exhibit a spherical morphology assembled from nano-building blocks, while the detailed morphology of each sample depends on the solvothermal temperature. The CuS-120 sample (Figure 3.13 a) displays spheres composed of thin, randomly oriented nanosheets, resulting in a highly porous structure. Upon increasing the solvothermal temperature, the CuS-150 sample (Figure 3.13 b) shows nanosheets that are considerably thicker than those of CuS-120; these nanosheets also assemble randomly into spheres. A further increase in solvothermal temperature leads to spheres with smoother surfaces, as the nanosheets continue to thicken and fully cover the sphere surface, thereby reducing the porosity compared to the other two samples. This result indicates that increasing the solvothermal temperature causes the nanocrystals to agglomerate into larger crystalline blocks. TEM images

(Figure 3.13 d-f) further confirm that all three CuS materials have a homogeneous spherical morphology.

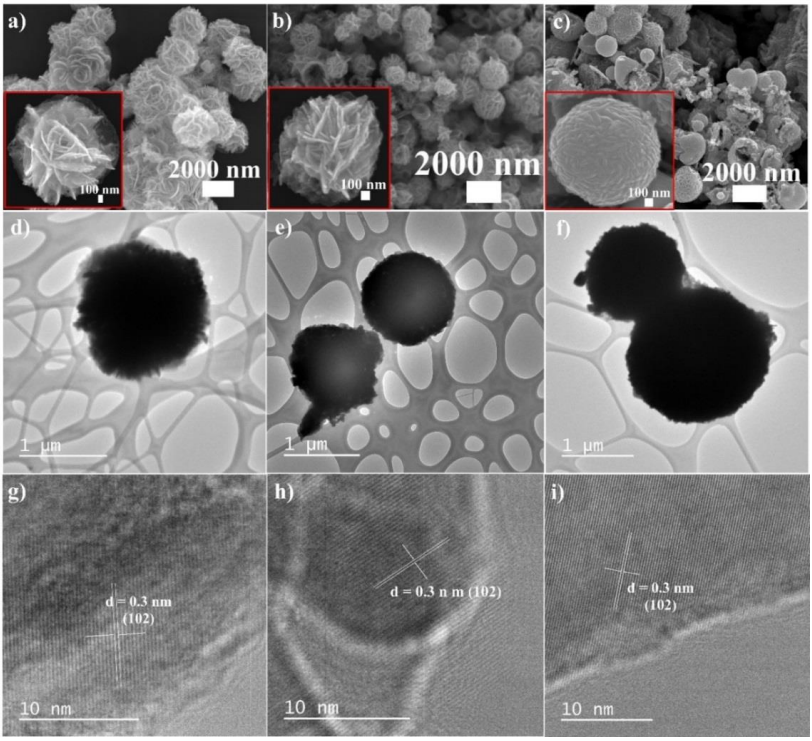

Figure 3.13. *Scanning electron microscopy (SEM) images of CuS materials synthesized by the solvothermal method at different temperatures: a) 120 °C, b) 150 °C, c) 180 °C.*

High-resolution TEM images (Figure 3.13 g-h) show clearly observable lattice fringes with an interplanar spacing of 0.3 nm, as measured by ImageJ software. This spacing corresponds to the (102) plane of the hexagonal structure of CuS. Notably, compared to the CuS-120 and CuS-180 samples, the CuS-150 sample exhibits a distinct feature in the HRTEM images: it shows regions with distorted lattice fringes and uneven contrast, indicating the coexistence of both ordered and disordered nanoscale domains within the CuS-150 sample. For the CuS-120 sample, only short lattice fringes are observed, whereas the CuS-180 sample shows long, well-defined fringes, consistent with a more perfect crystal structure formed at the higher synthesis temperature.

3.3.4. Product selectivity of the reduction process on the CuS material

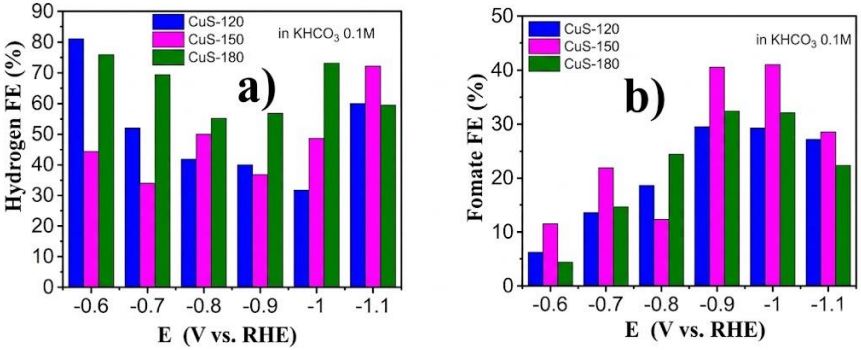

Figure 3.14. *Faraday efficiency of CuS materials synthesized by the solvothermal method at different temperatures (120, 150, 180 °C) at various potentials (from –0.6 to –1.1 V vs. RHE) in CO_2-saturated 0.1 M $KHCO_3$ solution for the products: a) Hydrogen; b) Formate.*

To evaluate the product selectivity of the CuS materials, the electrodes were electrolyzed in CO_2-saturated 0.1 M $NaHCO_3$ solution at potentials of -0.6, -0.7, -0.8, -0.9, -1.0, and -1.1 V *vs.* RHE. Over 2 hours, the catalytic current density did not decrease significantly, indicating that the CuS catalysts are rather stable for the electrochemical CO_2 reduction reaction. Figure 3.14 shows the Faraday efficiency of the CuS materials at different potentials for the main products: hydrogen and formate. These results are consistent with density functional theory (DFT) calculations and Raman spectroscopic measurements, which indicate that CuS_x materials exhibit high selectivity for the $HCOO^-$ product. At low potentials (-0.6, -0.7 V), the main product is H_2, with a Faraday efficiency exceeding 80% for the CuS-120 material at -0.6 V *vs.* RHE. As the potential increases to -0.9 and -1.0 V *vs.* RHE, H_2 production decreases while formate ($HCOO^-$) production increases; the Faraday efficiency for $HCOO^-$ rises significantly (from 30% to 41.2%) for all materials. The highest formate Faraday efficiency (41.2%) is achieved by the CuS-150 material. This is consistent with the LSV results, where CuS-150 exhibited the best electrochemical activity. Upon further increasing the potential to –1.1 V *vs.* RHE, the Faraday efficiency for $HCOO^-$ decreases for all three materials. This demonstrates that both the material morphology and the applied potential strongly influence the product efficiency, and that CuS-150 produces the highest amount of $HCOO^-$.

3.3.5. Morphological and structural characterization of the CuS material after catalytic operation

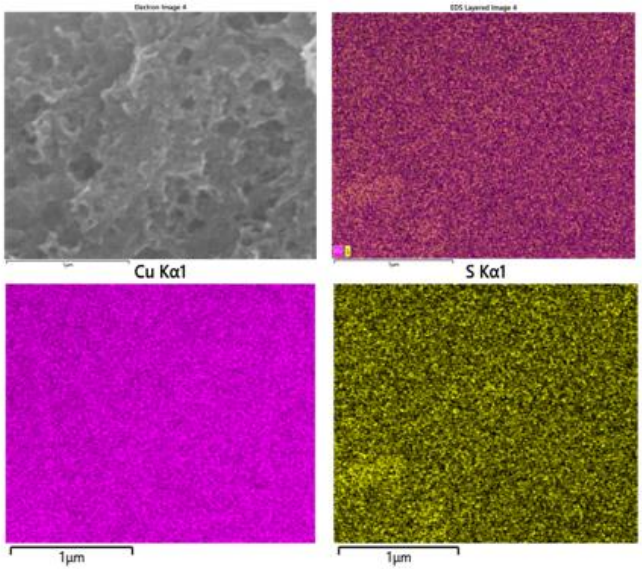

Figure 3.15. *EDS mapping results of the CuS-150 materials after 2 h of electrolysis in CO_2-saturated 0.1 M $KHCO_3$ solution at –1.0 V vs. RHE.*

After electrolysis, the surface was predominantly composed of Cu, with only a few spots showing the presence of S (EDS mapping results, Figure 3.15). The uniform dispersion of Cu and S observed initially was no longer present. EDX analysis revealed that Cu accounted for 94–95% of the surface, while S accounted for only 4–6%. This indicates that the CuS material on the surface had transformed to form metallic Cu.

CONCLUSIONS

This thesis was undertaken with the objective of synthesizing electrocatalytic materials for the CO_2 reduction reaction. To this end, several Cu-based catalysts, namely CuO, CuS, and $Cu_xFe_{3-x}O_4$ (CFO) spinel, were fabricated and systematically investigated in terms of their structure, morphology, and product selectivity for the electrochemical CO_2 reduction, as well as their post-electrolysis transformations. Based on the experimental findings, the main conclusions are summarized as follows:

1. CuO materials were synthesized by the sol-gel method at different calcination temperatures (400, 600, 800 ^oC). The results show that the calcination temperature markedly affects the morphology and crystallinity of the materials. Among them, CuO-400 (calcined at 400 °C) possesses small particle size and high grain boundary density, exhibiting the best catalytic activity with a Faraday efficiency (FE) of 26% for formate ($HCOO^-$) at -0.9 V *vs.* RHE. This is attributed to the fine particle structure, which facilitates CO_2 adsorption and activation, thereby promoting the formation of organic products (formate and acetate).

2. Spinel $Cu_xFe_{3-x}O_4$ materials (with x = 0.5, 1, 1.5, 2) were also successfully synthesized by the sol-gel method. They exist as mixed phases of $CuFe_2O_4$ spinel with either CuO or Fe_2O_3. Notably, these materials exhibit very high selectivity for the hydrogen evolution reaction (HER), with FE reaching nearly 100% for CFO-1 and CFO-1.5 at -0.6 and -0.7 V *vs.* RHE. In addition, CFO-1 shows an ability to produce acetate with the highest FE of 4.5%, demonstrating the role of the spinel structure in C-C bond formation.

3. CuS materials were prepared by the solvothermal method at 120, 150, and 180 °C. Among them, CuS-150 (synthesized at 150 °C) exhibits superior activity, giving the highest current density (-1.4 mA/cm^2 at -0.8 V after 10 cycles) and the highest selectivity for formate with an FE of 41.2% at –1.0 V *vs.* RHE. This is the highest formate FE among all the materials studied, confirming the potential of sulfide-based materials for directing the electrochemical CO_2 reduction toward formate.

4. Comparison of the selectivity of the catalysts synthesized in this thesis reveals: For H_2 gas, the spinel $Cu_xFe_{3-x}O_4$ materials show the highest selectivity, with FE up to ~100% for CFO-1 and CFO-1.5 at -0.6 and -0.7 V *vs.* RHE; for formate, CuS-150 exhibits the highest selectivity with an FE of 41.2% at -1.0 V *vs.* RHE, while CuO-400 gives an FE of about 26% at -0.9

V *vs.* RHE; for acetate, the CFO-1 spinel material shows the highest selectivity with an FE of 4.5% at -0.6 V *vs.* RHE.

5. Investigation of the structure and morphology of the catalysts after electrolysis shows that CuO and CuS are completely converted into metallic copper (Cu^0) – the true active site for the CO_2 reduction reaction. In contrast, the $Cu_xFe_{3-x}O_4$ spinel materials are partially reduced to metallic iron (Fe^0), while the remaining spinel structure plays a key role in catalyzing C-C bond formation to produce acetate. These results provide a scientific basis for explaining the differences in product selectivity among the materials. Based on these findings, the active sites for the CO_2 reduction reaction on each material have been proposed.

NEW CONTRIBUTIONS OF THE THESIS

This is the first study in Vietnam to investigate three copper/iron-based catalysts (CuO, CuS, and $Cu_xFe_{3-x}O_4$ spinel) for the electrochemical CO_2 reduction reaction (CO_2RR), and provides a reliable dataset on Faraday efficiency and product selectivity for each catalyst:

1. CuO (synthesized by the sol-gel method using agar as a gelling agent): the effect of calcination temperature on structure was investigated by different techniques (XRD, SEM-EDX, FT-IR). The products of CO_2RR on CuO electrodes are H_2, formate, acetate, and CO.

2. $Cu_xFe_{3-x}O_4$ spinel (synthesized by the sol-gel method): the effects of the Cu^{2+}/Fe^{3+} molar ratio and calcination temperature on structure were studied by different techniques (SEM-EDX, TEM, XRD, Raman, FT-IR, XPS). The main products of CO_2RR are H_2, formate, and acetate.

3. CuS (synthesized by the solvothermal method): the influence of synthesis temperature on structure and morphology was investigated by XRD, Raman, SEM-EDX, XANES, EXAFS, TEM, HR-TEM. All the products of CO_2RR are H_2 and formate.

LIST OF THE PUBLISHED PAPERS RELATED TO THE DISSERTATION

1. ***Xuan T. Mai,*** Tuan M. Duong, Duc N. Nguyen, Tung H. To, Hoang H. Luc, Phong D. Tran, and Ly T. Le, "Sol–Gel Synthesis of CuO Nanoparticles and Its Use as Catalyst for Electrochemical CO_2 Reduction", Energy Technol. 2024, 2401486 (ISI, IF 3.6).
2. ***Xuan T. Mai***, Hoang H. Luc, Phong D. Tran, Ly T. Le, "Sol-Gel Synthesis of Copper Ferrite Spinel Oxide and Its Use as Catalyst for the H_2 Evolution and CO_2 to Acetate Reduction Reactions", ChemistrySelect 2025, 10, e00515 (SCIE, IF 2.0).